Sustainable Precision Machining of Nimonic 90 Alloy with Biodegradable B_4C-Enriched Dielectric in Micro-EDM

Sahil Sharma[1*], Sukhdeep Singh[1], Shivam Kumar[1], Shubhashit Chowdhury[1]

[1]Department of Mechanical Engineering, School of Engineering and Technology, CGC University, Mohali-140307, Punjab, India
*corresponding author: sahil.j2863@cgcuniversity.in

Abstract

The study explores the application of coconut oil-based biodegradable dielectric fluid enriched with boron carbide (B_4C) nanoparticles in micro-electric discharge machining (micro-EDM) of Nimonic 90 alloy. Experiments were designed using response surface methodology (RSM) with a central composite design to evaluate the effects of pulse-on time, current, and powder concentration on material removal rate (MRR) and average surface roughness (ASR). The results revealed that discharge current had the highest influence on MRR, while pulse-on time was the most significant factor for ASR. Optimal machining conditions of 60 µs pulse duration, 20 A current, and 15 g/L B_4C concentration achieved a maximum MRR of 0.0271 g/min and a minimum ASR of 3.15 µm. Microstructural analysis through SEM confirmed the presence of recast layers, microcracks, and voids, with improved surface integrity under optimized conditions. The integration of coconut oil with B_4C nanoparticles not only enhanced machining performance but also demonstrated environmental benefits, cost-effectiveness, and sustainability compared to conventional hydrocarbon-based dielectrics. These findings highlight the potential of bio-based nanofluid dielectrics as an eco-friendly and efficient alternative for precision machining of nickel-based superalloys.
Keywords: Micro-EDM, Nimonic 90, Biodegradable dielectric, Surface integrity, Sustainable machining

1. Introduction

Electric discharge machining (EDM) is an unique technique that is frequently used to easily remove or manufacture extremely hard materials and complex geometries that would otherwise be impossible with the use of conventional techniques of machining like turning, milling and drilling. Problems with immoderate wear, less material removal rate (MRR), inadequate surface finish emerged when sophisticated materials like superalloys, ceramics and composites were processed using traditional machining techniques. But with advent of non-conventional machining techniques, which provide greater accuracy and precision than conventional techniques, the issues with conventional machining techniques were resolved [1-2]. EDM is a material removal technique that ionizes the dielectric fluid present in the tool-workpiece gap by repeatedly sparking, producing significant thermal energy [3-5]. The intensity of the discharge eventually creates a plasma channel that serves as a powerful heat source. The formed plasma channel, which has a tendency to vaporize or melting of particles from the surface of the workpiece material, is the origin of

V. Kumar et al. (eds.), *Proceedings of the International Conference on Advanced Design, Manufacturing, and Sustainable Energy Systems (ICADMSES 2026)*, Atlantis Highlights in Engineering 45,
https://doi.org/10.2991/978-94-6239-750-7_5

localized heating [6]. The degraded materials are melted and vaporized with the help of a sequence of electric sparks, which raises the temperature to about 8000°C to 12,000 °C. With the aid of dielectric fluids directed toward the cutting zone, the debris covering the specimen is subsequently pushed away [7-8].

EDM fluids including hydrocarbon oil, kerosene, EDM oil etc emit hazardous gasses during machining, posing substantial environmental and health risks. In the EDM process, addition of ceramic nanoparticles to the dielectric improves machinability by enhancing removal rate, surface integrity and decreasing tool wear rate. Nimonic-90 is an alloy composed of Ni-Co-Cr that is utilized at high temperatures in the field of defence, aerospace, marine and power generation industries. It is used to make various elements such as jet engines, exhaust re-heaters, ring sections, turbine blades due to its strong mechanical qualities which include exceptional resistance to corrosion, high creep and fracture strength [9-10]. The influence of different tool materials on powder mixed EDM of a nickel-based superalloy, Nimonic 75 along with using three different powders (zinc, Co and Mo). Tool wear rate (TWR), material removal rate (MRR) and surface roughness (R_a) was estimated by L27 3^{13} Taguchi approach on EDM using control parameters. Peak current was found as greater influencing parameters for MRR, TWR and R_a. Highest MRR observed at mixing of zinc powder in dielectric and Mo powder for surface finish [11]. The enhancement in surface quality of Monel K500 alloy has been investigated by using coconut oil as dielectric in wire-cut EDM process. The Taguchi array (L27) array was used to test responses such as wear rate of wire and kerf width [12]. The surface integrity of machined surface is greatly enhanced by nanomaterials like SiO_2 and Al_2O_3 embedded in the dielectric fluid. A mixture of Al_2O_3 (75%) and SiO_2 (25%) demonstrated in reduced EWR and increased MRR [13].

However, minimizing waste material and cutting down on experimental duration require forecasting and optimization of machining factors which improves process effectiveness and utilization of resources in manufacturing processes. While many studies have focused on improving machining quality and efficiency in materials like Ti alloy, Al 5083, AISI H13 steel, and Monel-K500 alloy. Green EDM process adopted [14] to analyze the performance of various input machining factor such as duty factor, voltage, current and electrode material on machining output variables viz. MRR, Ra, residual stress and white layer thickness (WLT) during EDM operation of alpha-Beta Titanium alloy. The modification in the process had done by mixing ordinary water into deionized water to make it eco friendly and sustainable EDM process. The significant parametric combination was found with integrated model of Taguchi and Grey-Relational analysis (TGRA). The experimentation and analysis of results shows that mechanism of material erosion with mixed dielectric medium performed better due to high thermal conductivity of insulating dielectric medium. The impact of sunflower dielectric on roughness, MRR and electrode wear rate (EWR) during EDM of Inconel 800 has also been examined [15]. The outcome proved that using sustainable oil as a dielectric rather than kerosene leads to rise in MRR. Furthermore, EWR and roughness results were also significantly provides better performance with sunflower compared to kerosene oil. It has also asserted that eco-friendly oils serves as a superior alternate to hydrocarbon-based dielectrics because of its improved and comparable dielectric qualities. The potential of Pongamia oil for sustainable EDM of Inconel 718 alloy has been explored [16]. The defined set of input characteristics was used to assess various responses such as TWR, MRR and Ra. The results revealed that vegetable oil indicated above may take the place of traditional EDM dielectric since it produced excellent machining results. Additionally, the feasibility of using Polanga oil as a dielectric fluid for machining of EN 31 tool steel has been investigated [17].

Nanomaterials based on ceramics have shown promise in raising MRR while preserving a tolerable level of surface roughness. Although several studies have investigated powder-mixed EDM (PM-EDM) of nickel-based superalloys such as Nimonic 80A and Inconel variants using metallic or oxide powders in hydrocarbon-based dielectrics, limited attention has been given to sustainable micro-EDM of Nimonic 90 alloy using biodegradable dielectric media. Existing PM-EDM studies primarily focus on performance enhancement, often overlooking environmental impact, dielectric biodegradability, and green manufacturing aspects. Moreover, the combined influence of coconut-oil-based dielectric and ceramic B_4C powder on micro-scale machining characteristics such as material removal rate (MRR), aspect ratio stability (ASR), and surface integrity of Nimonic 90 has not been systematically explored.

2 Materials and methodology

According to the previous research, EDM process using kerosene oil can produce dangerous vapours that have detrimental effects on machine operator's health and surrounding environment [18–20]. The suggested feasible EDM with controllable variables are used to process magnesium alloy in the current study. In the first phase, particles of boron carbide (B_4C) blended with coconut oil, and the process of machining is carried out in second step. Nimonic 90 (nickel based alloy) has been selected as a workpiece material for the present study. Copper electrode 99.9% of diameter 10 mm is used as a tool electrode. The chemical composition of selected superalloy and copper electrode are shown in the Table 1 and Table 2 respectively. The mechanical properties of Nimonic 90 have been illustrated in Table 3. Schematic diagram of machined surface of workpiece material shown in the Fig.1(a) and Machining tool electrode shown in Fig.1(b). Table 4 elaborates on the prominent attributes of all the biodegradable oil. Boron carbide (B_4C) nanopowders were employed as suspended material with a mean powder size of 100 nm.

Table 1. Chemical distribution of Nimonic 90 alloy

Element	C	Si	Mn	S	Cu	Ni	Cr	Co	Al	Ti	Zr	Fe
Composition (wt%)	0.12	0.26	0.37	0.01	.085	remainder	18.8	15.96	1.113	2.223	0.06	0.48

Table 2. Chemical distribution of Copper electrode

Element	C	Sn	Ni	S	C	Zn	Al	P	Pb

Composition (wt%)	99.5	0.006	0.03	0.05	0.04	0.19	0.006	0.04	0.06

Table 3. Mechanical properties of Nimonic 90

Property	value
Thermal conductivity	12.78 W/m°C (at 100°C)
Melting range	1370°C (liquidus temp.)
Electrical resistivity (at 20°C)	1.17 µohm•m
Density	8.19 g/cm³ (in metric)
Tensile strength (Ultimate)	910-1028 MPa (at 650°C)
Hardness	290 HV

Table 4. Properties of biodegradable dielectricc oil

Biodegradable oil	Viscosity (centipoise) at 25°C	Dielectric strength (KV/mm)	Flash point (°C)
Coconut oil	50-60	25-35	245

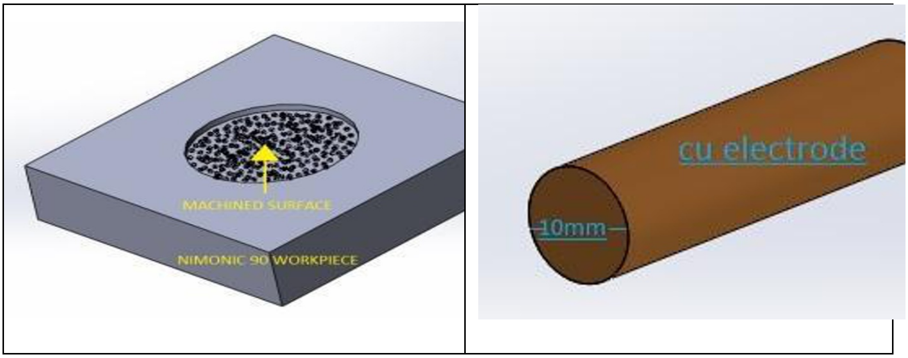

Fig 1. (a) Schematic diagram of Work piece material (Nimonic 90) with EDMed surface and (b) machining tool electrode (copper)

The schematic diagram of EDM for micromachining process which includes D.C power supply, current control, servo control, workpiece and electrode immersed in the dielectric fluid is displayed in the Figure 2. The experiments are carried out on a die-sinking EDM setup (Model G30, Make: Press Mach. Machine Tools) as illustrated in Figure 3. The size of the working table is 350 x 220 mm. Machine travel stroke range is 220 x 130 mm in longitudinal (X) direction and cross (Y) directions. For optimal consistency and minimize surface imperfections, a P2000 grit number emery paper was used to polish the upper surfaces of the workpiece and copper electrode. Using response surface methodology (RSM), the tests were conducted under a variety of parametric settings. The different levels were selected for machining of Nimonic 90 alloy used in the present investigation is shown in the Table 5. The conducting electrode and workpiece were immersed in a B_4C-enriched insulating fluid during EDM process. The vaporization and melting of workpiece material was caused by extreme localized temperatures produced by the spark produced by EDM process within the machining zone. A constant machining duration of 10 minutes was selected for each experimental run based on preliminary trials, which indicated that this duration ensured stable discharge conditions, minimized transient effects during initial tool-workpiece engagement, and produced sufficient machining depth for reliable evaluation of MRR and ASR. The pressurized dielectric medium was then used to flush the molten waste particles out of the machining zone. The enhancement may occur in electric and thermal conductivity of coconut dielectric by the addition of B_4C nanoparticles.

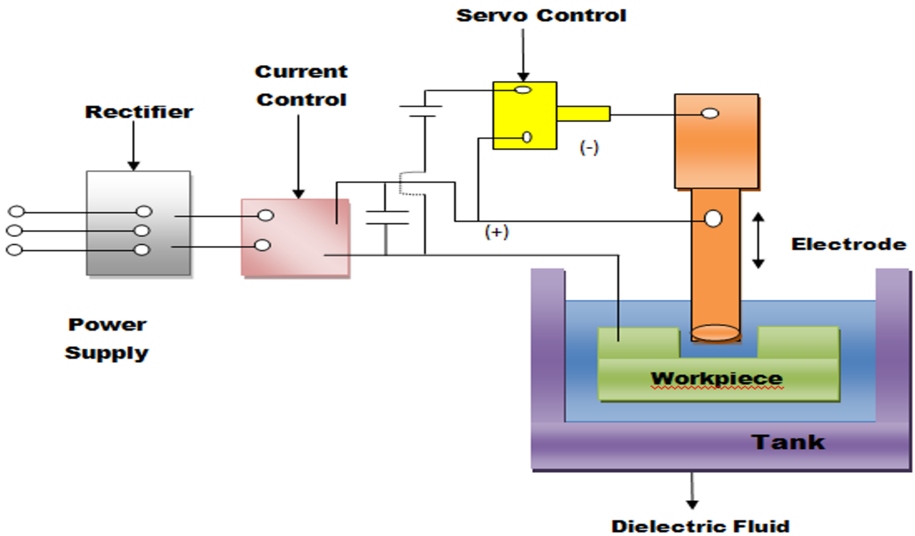

Fig 2. Schematic diagram of an EDM setup used for micromachining

Fig 3. EDM used for experiments.

Material removal rate (MRR) and average surface roughness (ASR) are two essential responses that are primarily analyzed in the performance evaluation of EDM. The rate at which material has been removed from the workpiece during machining can be used to explain MRR. The formula found in Equation 1 can be used to compute it in g/min.

$$MRR = \frac{W_i - W_f}{t} \quad (1)$$

where,
W_i = workpiece's material weight before cutting (gm)
W_f = workpiece's material weight after cutting (gm)
t = cutting duration (min)

Average surface roughness (ASR) is the most commonly used parameter to analyse the roughness of the material's surface. It is also known as the arithmetic average or centre line average (CLA). In terms of mathematics, R_a is the arithmetic mean of the sample length's absolute deviation of the profile from the reference line. The average roughness, or R_a value across a single sampling length, ensures that the effects of non-typical peaks and valleys are averaged out and do not significantly affect the outcomes. Average surface roughness (R_a) of all work surfaces were recorded by Tele Surf SJ-201 ranges of 350μm (-200μm to +150μm). The values of the responses (MRR and ASR) have been depicted in Table 6.

Table 5. Machining parameters with different level

Input Parameters	Notation	Level difference

		-2	-1	0	+1	+2
Pulse-on time (µs)	A	20	40	60	80	100
Current (Amp)	B	4	8	12	16	20
Powder Concentration (g/L)	C	6	9	12	15	18

Table 6. Design for central composite: various controlling factors and results

Expt No.	Input Variables			Responses	
	A	B	C	MRR (g/min)	ASR (µm)
1	-1	-1	-1	0.0154	4.615
2	1	-1	-1	0.0162	5.741
3	-1	1	-1	0.0179	4.989
4	1	1	-1	0.0225	5.812
5	-1	-1	1	0.0165	4.034
6	1	-1	1	0.0171	5.363
7	-1	1	1	0.0215	4.578
8	1	1	1	0.0239	5.912
9	-2	0	0	0.0175	4.262
10	2	0	0	0.0204	6.413
11	0	-2	0	0.0167	5.157
12	0	2	0	0.0286	6.287
13	0	0	-2	0.0183	6.143
14	0	0	2	0.0211	5.965
15	0	0	0	0.0197	5.462
16	0	0	0	0.0204	5.865
17	0	0	0	0.0194	5.514
18	0	0	0	0.0199	5.667
19	0	0	0	0.0207	5.834
20	0	0	0	0.0197	5.956

3. Results and Discussion

Response surface methodology (RSM) is a quantitative and mathematical tool used to improve the process of optimization. It is commonly used to explore the link between numerous variables and their associated responses [21]. In this study, design of central composite was used to arrange the experiments since it has been effective at optimizing the process variables with some runs of experiment while assuring robust statistical evaluation. This composite design is an ideal for analyzing how numerous variables, including, on time (T_{on}), current and powder concentration, affect roughness and MRR. The mathematical explanations for both MRR and ASR were developed using experimental data. The regression equations for MRR and ASR are shown in Eqs. (2) and (3) respectively

$$MRR = 0.019705 + 0.000888\,A + 0.002775\,B + 0.000788\,C - 0.000385\,A*A + 0.000540\,B*B - 0.000198\,C*C + 0.000700\,A*B - 0.000300\,A*C + 0.000375\,B*C \quad (2)$$

$$ASR = 5.611 + 0.557\,A + 0.237\,B - 0.102\,C - 0.1472\,A*A - 0.0510\,B*B + 0.0320\,C*C - 0.037\,A*B + 0.089\,A*C + 0.081\,B*C \quad (3)$$

ANOVA was used to analyze the relevance and percentage contribution provided by each factor in the models, identifying the most significant characteristics for MRR and ASR. The F-value is an indicator of statistics used to assess model and parameter relevance. It is computed by dividing the mean sum of squares of the variables in the model by the mean sum of squares of the experimental error [22]. The constructed model was relevant for analyzing MRR and ASR, as indicated by F-values with a lack of fit. The models' statistical importance and appropriateness for predicting both responses have been verified by p-values of less than 0.05 at a 95% confidence level. ANOVA results for MRR and ASR are shown in Tables 7 and 8, respectively. The average absolute error (percentage) for MRR and ASR was found to be 4.79% and 5.36%, respectively, demonstrating high prediction accuracy. Tables 7 and 8 demonstrate a lack of fit for MRR and ASR at 9.01 and 7.72 respectively. The low lack-of-fit values show that model accurately describes information from the experiments. Figure 4 shows the normal probabilistic graphs for MRR and ASR. The residuals are uniformly placed on diagonal path, indicating that the model of regression adequately captures the experimental data and meets its assumptions. The linear impact analysis revealed that current was the most significant factor for MRR with 68.71% contribution and pulse on time (T_{on}) exhibits maximum contribution for ASR with 57.79%. The square-effect assessment revealed that current had the largest percentage contribution to MRR with 3.91% and T_{on} has maximum contribution of 6.33% to ASR. The interaction of on-time and current' resulted in the highest MRR with contribution of 2.24%, whereas the interaction of on-time and PC contributed 0.74% to ASR.

3.1 Effect of Parameters on MRR

Figure 5 shows how machining parameters affect MRR during EDM of Nimonic 90 alloy. As current increases from 4A to 20A, MRR increases gradually and reaches a peak of 0.0286 g/min. The higher discharge energy at 20A causes localized vaporization and melting of surface material, resulting in efficient removal of material. This is to be expected since a stronger spark generated by a rise in pulse current raises the temperature, which in turn causes more material to melt and erode away from the workpiece [23]. Additionally, the higher value of discharge current produces uncertain machining circumstances, resulting in unfavorable impacts such as high electrode wear and lower efficiency of MRR. The combined effects of pulse-on time, discharge current, and B_4C powder concentration significantly influence plasma channel expansion and heat flux distribution during micro-EDM. Increased Ton and current enhance spark energy, resulting in higher localized temperatures and intensified melting and vaporization. The presence of B_4C particles reduces dielectric breakdown strength, promoting wider plasma channels and uniform energy dispersion. This leads to controlled material removal, reduced thermal gradients, and improved surface integrity, as evidenced by SEM observations.

Table 7. ANOVA result for MRR

Source	DF	Adj SS	Adj MS	F-Value	P-Value
Model	9	0.000167	0.000019	15.51	0.000
Linear	3	0.000146	0.000049	40.66	0.000
A	1	0.000013	0.000013	10.55	0.009
B	1	0.000123	0.000123	103.12	0.000
C	1	0.000010	0.000010	8.30	0.016
Square	3	0.000015	0.000005	4.27	0.035
A*A	1	0.000004	0.000004	3.12	0.108
B*B	1	0.000007	0.000007	6.13	0.033
C*C	1	0.000001	0.000001	0.82	0.386
2-Way Interaction	3	0.000006	0.000002	1.61	0.249
A*B	1	0.000004	0.000004	3.28	0.100
A*C	1	0.000001	0.000001	0.60	0.456
B*C	1	0.000001	0.000001	0.94	0.355
Error	10	0.000012	0.000001		
Lack-of-Fit	5	0.000011	0.000002	9.01	0.015
Pure Error	5	0.000001	0.000000		
Total	19	0.000179			

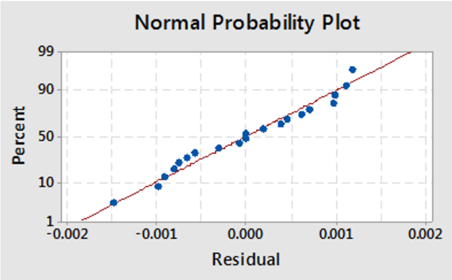

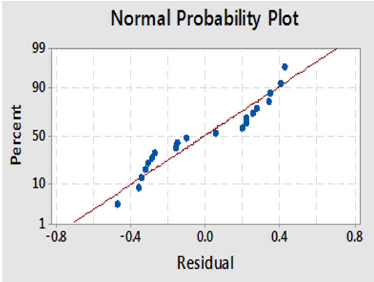

Fig 4. Normal probability plot for **(a)** MRR and **(b)** ASR models.

As pulse on time increases from 20 µs to 60 µs, the MRR increase significantly. The peak value of 0.0211 g/min was attained at an intermediate T_{on} of 60 µs. At increasing T_{on}, more discharge energy is produced between inter electrode gap leading in dissociation of dielectric fluid, therefore carbon particles were discharged. However, at higher level of T_{on} (80 µs), the value of MRR decreases due to high heat intensity, preventing efficient discharge of molten material [24]. The debris present in the spark gap can interfere with the EDM process, lowering its efficiency for removal of material. The powder concentration of B_4C plays critical role for enhancing the performance of machining in EDM. The maximum MRR value of 0.0207 g/min was achieved at a concentration of 12 g/L; the MRR significantly improves as the PC rises from 6 g/L to 12 g/L. This may be lead to an improvement in electric and thermal conductivity of dielectric medium [25]. The addition of B_4C helps in stabilizing the discharge of electricity and transferring energy to workpiece material, resulted in enhancing material expulsion. At 15 g/L, MRR drops due to increased density of particles in the dielectric fluid. This reduces flushing performance and causes spark instability due to an accumulation of particles [26]. The accumulated particles might impede the spark gap, limiting discharge performance and lowering MRR.

Table 8. ANOVA result for ASR

Source	DF	Adj SS	Adj MS	F-Value	P-Value
Model	9	6.83671	0.75963	4.32	0.016
Linear	3	6.03300	2.01100	11.45	0.001
A	1	4.96621	4.96621	28.27	0.000
B	1	0.90155	0.90155	5.13	0.047
C	1	0.16524	0.16524	0.94	0.355
Square	3	0.67640	0.22547	1.28	0.333

A*A	1	0.54449	0.54449	3.10	0.109
B*B	1	0.06548	0.06548	0.37	0.555
C*C	1	0.02569	0.02569	0.15	0.710
2-Way Interaction	3	0.12731	0.04244	0.24	0.865
A*B	1	0.01110	0.01110	0.06	0.807
A*C	1	0.06372	0.06372	0.36	0.560
B*C	1	0.05249	0.05249	0.30	0.597
Error	10	1.75667	0.17567		
Lack-of-Fit	5	1.55523	0.31105	7.72	0.021
Pure Error	5	0.20145	0.04029		
Total	19	8.59339			

3.2 Effect of parameters on ASR with microstructure analysis

Figure 6 depicts the effects of pulse-on time (T_{on}), current (I) and powder concentration (PC) on surface roughness (ASR). Such variables are critical for identifying the discharge power, temperature distribution and material removal technique used in the EDM process. Together, they have a direct impact on the formation of microstructural imperfections. As a result, a detailed study of these the variables are critical for assessing ASR outcomes post-EDM. It has been found that increasing the current (I) from 4A to 12A enhanced the surface roughness (ASR). However, when the current was raised to 16A, the ASR gradually starts reducing. At 4A, the MSR measured 5.36 μm, indicating a modest value of roughness. This pattern of behaviour is most likely owing to the minimized discharge energy at 4A, which encourages a more controlled and steady material removal process [27]. When Ton increases, roughness of the surface rises until it reaches at maximum value of 6.41 μm. Increases in pulse-on time resulted in increased total energy provided to the workpiece, which causes more material to be eroded from its surface, raising the workpiece's surface roughness (R_a). However, when T_{on} increases, the plasma that forms between electrode gaps obstructs energy transfer, forming tiny craters as a result, which lowers R_a.

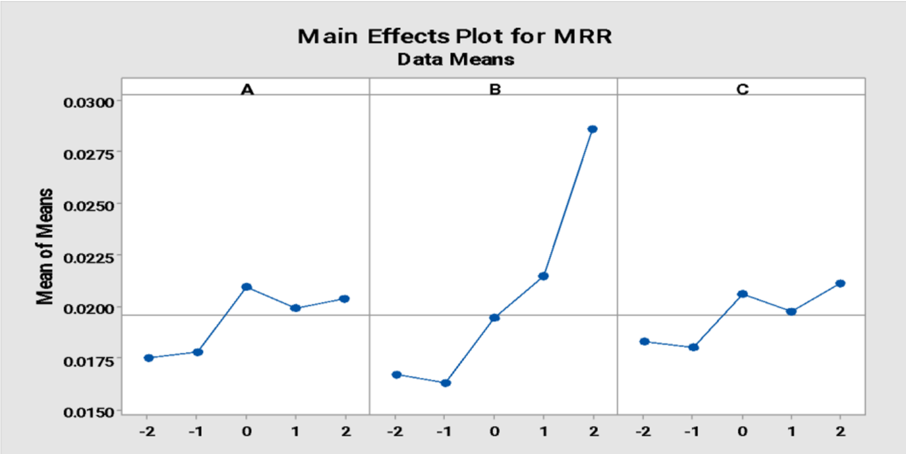

Fig 5. Main effect plot for MRR

Low discharge energy additionally generates insufficient heat to adequately erode particles from the surface of workpiece material. As a result, the end outcome may be less finished. Furthermore, the limited energy precludes efficient draining of melted debris from the machining region, resulting in discrepancies like pores and craters [28]. When current (I) is increased to 20A, the roughness value increases marginally to 6.28 µm, resulting in a deterioration in surface quality. While increased current improves particle removal effectiveness and it also generates an excessive amount of heat. This increased thermal energy causes the formation of a recast layer on the machined surface, as well as thermal strains and the generation of microcracks, as illustrated in Figure 7.

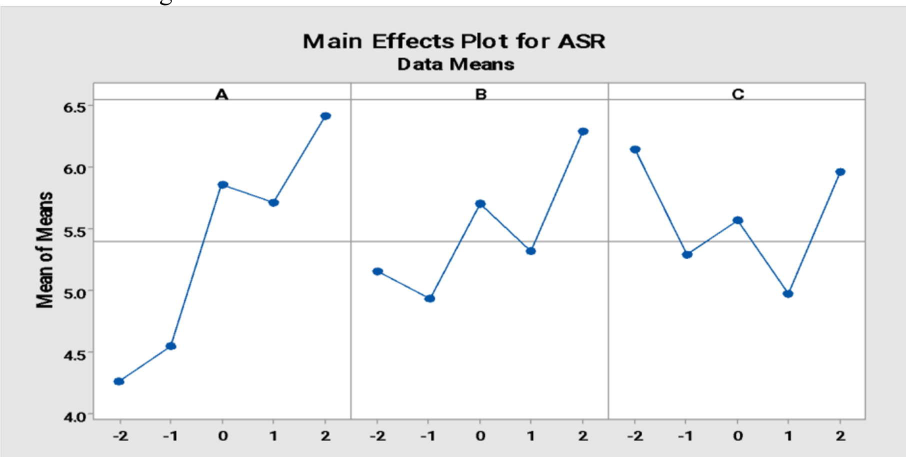

Fig 6. Main effect plot for ASR

The existence of these imperfections at 20A increases the value of ASR which leads in reduction of machined surface quality. At 8A, ASR reached its most minimal recorded value of 4.93 µm among all five current values. This is mainly because of the discharge energy at 8A is considerably larger, essentially melting and vaporizing the workpiece material [29], increasing the rate of particle removal. Furthermore, the rising temperature input promotes the break down and discharge of molten particles, reducing the creation of the recast layer and minimizing microstructural defects. Higher current is often associated with rougher finished surfaces because to increased recast layer deposition and related thermal stresses, however this impact can be minimized under certain situation [30]. The decreased roughness found at 8A is essentially the result of greater discharge energy and effective particle ejection. This synergy promotes more uniform machining and results in a significant reduction in surface imperfections.

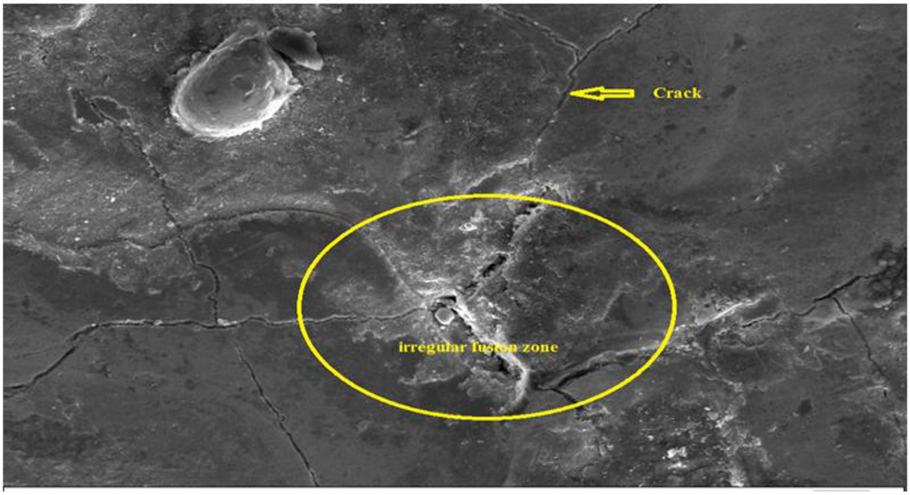

Fig 7. Effect of current on SEM micro cracks at 20A (at 1000X)

At a T_{on} of 20 µs, the observed material roughness was 4.26 µm. Such short pulse duration reduces plasma channel stability, leading to intense but uneven formation and collapse cycles. This instability causes irregular material removal from the work surface due to inconsistent energy discharge across the machining zone. The lower spark intensity at this short Ton inhibits uniform particle erosion, thereby contributing to the formation of a thin white recast layer on the machined surface, as shown in Figure 8. Energy-dispersive X-ray spectroscopy (EDS) was used to determine the elemental composition of the recast layer. The investigation confirmed the presence of chromium (Cr), copper (Cu), cobalt (Co), manganese (Mn), nickel (Ni), iron (Fe) and carbon (C), as well as a significant amount of oxygen. The identification of these elements are shown in Figure 9.

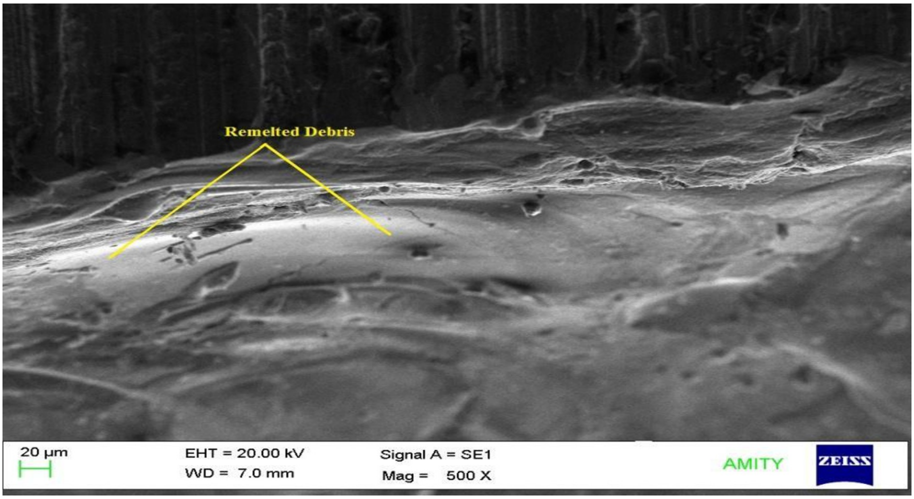

Fig 8. Effect of ‘T_{on}’ on SEM recast layer at 60µs (at 500X)

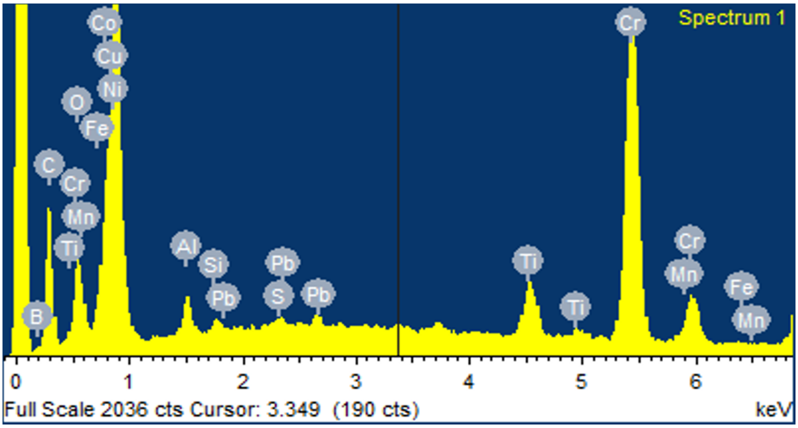

Fig 9. EDS result of recast layer

Furthermore, the short time available for plasma channel stabilization limits the effective removal of detritus from the inter-electrode gap. This results in a relatively rough machined surface. Raising the pulse-on time (T_{on}) to 60 µs resulted in a modest rise in the ASR value to 5.83 µm, but also a marginal loss in surface finish quality. During this stage, the plasma channel remains stable for an extended period, allowing for higher energy absorption at the intersection zone within the tool electrode and the workpiece [31]. While this situation promotes better melting of the material, it also causes precise overheating and fluctuations in spark energy. The ASR was lowered to 5.67 µm with an 80 µs pulse-on time, resulting in an improved surface quality. The greater pulse length encouraged the plasma channel to achieve complete stability, resulting in homogeneous energy supply throughout the manufacturing zone. This stability increases the effectiveness of clearing debris while also ensuring uniform particle erosion. At the same time, the spark intensity reaches an ideal point, decreasing the possibility of recast layer development and avoiding arcing, which is often caused by high heat and debris [32].

At a particle concentration of 15 g/L, the ASR was observed at 4.98 μm, indicating the best surface finish among all five tested values. This concentration provides a balanced particle density, allowing for the effective evacuation of molten debris from the spark gap while maintaining plasma channel stability [33]. The steady plasma channel allows for optimum flow of energy to the workpiece surface, resulting in constant particle removal and better ASR. Furthermore, the larger amount of B_4C particles in the dielectric reduces the possibility of spark bridging and secondary discharges, which could otherwise produce in defects like voids or an irregular recast layer [34]. When powder concentration is increased to 18 g/L, ASR climbs to 5.86 μm, indicating a decrease in quality of the surface. At a given concentration, the dielectric medium has better conductivity for both heat and electricity, allowing for the creation of denser along with more uniform sparks [35]. While localized sparks improve particles removal efficiency, it also increases possible risks of overheating on the workpiece surface [36]. Furthermore, a larger powder concentration in the dielectric solution might cause agglomeration which obstructs the flushing mechanism and reduces machining stability. A high powder concentration in the dielectric fluid causes significant accumulation within the zone of machining, increasing the flow rate of the fluid and interfering in the integrity of plasma channel [37].

Compared to conventional hydrocarbon-based EDM oils reported in the literature, the coconut-oil-based B_4C mixed dielectric demonstrated comparable or improved MRR with reduced ASR and lower observable tool wear. Additionally, biodegradable dielectric media offer reduced environmental toxicity and improved operator safety. These findings indicate that sustainable dielectrics can achieve performance parity with conventional EDM oils while significantly enhancing environmental compatibility.

4. Conclusion

In this study, Nimonic 90 alloy was treated utilizing sustainable EDM with an electrolytic copper electrode operating in reverse polarity. The combination of coconut oil with varying amounts of B_4C nanoparticles improved machining efficiency by acting as a dielectric medium. The investigation used a central composite design within the context of response surface methodology (RSM) to assess the effects of pulse-on time (T_{on}), current (I) and powder concentration (PC) on MRR and ASR. The optimum settings of, 60 μs pulse duration, 20 A current and

15 g/L powder concentration resulted in a maximum MRR of 0.0271 g/min and a minimum ASR of 3.15 µm. The main effect graphs showed that increasing the pulse-on time (T_{on}), current (I) and powder concentration (PC) resulted in an increase in MRR, peaking at 60 µs, 20 A, and 12 g/L respectively. ASR first increased with increasing T_{on} and I but then decreased at 60 µs and 12 A. Surface roughness was found to be adequate at 40 µs, 8 A, and 15 g/L concentration. SEM studies revealed a variety of surface defects on the machined surface, including microcracks, recast layers, craters, and voids. The study found that using coconut oil bio-dielectric with a 12 g/L B_4C concentration significantly improved machining performance and surface integrity.

Along with increased machining efficiency, the use of coconut oil as a bio-dielectric fluid augmented with B4C nanoparticles offers various advantages over typical dielectric materials. These include reducing the environmental impact, providing economic benefits through the use of recycled waste resources, and promoting the general sustainability of EDM operations. The biodegradable properties of coconut oil aid in boosting green manufacturing practices. Furthermore, the superior thermal and electrical properties of B4C nanoparticles facilitate efficient energy transfer during machining, resulting in higher surface quality, fewer surface imperfections, and improved overall machining performance.

Acknowledgments. The author(s) received no financial support for the research, authorship, and/or publication of this article.

Disclosure of Interests. The author(s) declared no potential conflicts of interest with respect to the research, authorship, and/or publication of this article.

References

1. Rezaei Ashtiani, H.R., Zarandooz, R.: Microstructural and mechanical properties of resistance spot weld of Inconel 625 supper alloy. Int. J. Adv. Manuf. Technol. 84(1–4), 607–619 (2016).
2. Prihandana, G.S., Mahardika, M., Hamdi, M., Wong, Y.S., Mitsui, K.: Application of powder suspended in dielectric fluid for fine finish micro-EDM of Inconel 718. Int. J. Adv. Manuf. Technol. 75(1–4), 599–613 (2014).
3. Ishfaq, K., Asad, M., Anwar, S., Pruncu, C.I., Saleh, M., Ahmad, S.: A comprehensive analysis of the effect of graphene-based dielectric for sustainable electric discharge machining of Ti-6Al-4V. Materials 14(1), 23 (2020).
4. Sharma, S., Vates, U.K., Bansal, A.: Optimization of machining characteristics for EDM of different nickel-based alloys by embodying fuzzy, grey relational and Taguchi technique. World J. Eng. 18(1), 23–36 (2021).
5. Matsumoto, M., Umeda, Y., Masui, K., Fukushige, S.: Design for Innovative Value Towards a Sustainable Society: Proceedings of EcoDesign 2011: 7th International Symposium on Environmentally Conscious Design and Inverse Manufacturing. Springer, Dordrecht (2012).

6. Shabgard, M., Kakolvand, H., Seyedzavvar, M., Shotorbani, R.M.: Ultrasonic assisted EDM: Effect of the workpiece vibration in the machining characteristics of FW4 welded metal. Front. Mech. Eng. 6, 416–424 (2011).
7. Nahak, B., Gupta, A.: A review on optimization of machining performances and recent developments in electro discharge machining. Manufacturing Rev. 6, 2 (2019).
8. Das, S., Paul, S., Doloi, B.: Assessment of the impacts of bio-dielectrics on the textural features and recast-layers of EDM-surfaces. Mater. Manuf. Process. 36(2), 245–255 (2021).
9. Kumar, V., Jangra, K.K., Kumar, V., Sharma, N.: GA-based optimisation using RSM in WEDM of Nimonic-90: A nickel-based super alloy. Int. J. Ind. Syst. Eng. 28(1), 53–64 (2018).
10. Pandey, A.K., Gautam, G.D.: Grey relational analysis-based genetic algorithm optimization of electrical discharge drilling of Nimonic-90 superalloy. J. Braz. Soc. Mech. Sci. Eng. 40(3), 117 (2018).
11. Ramesh, S., Jenarthanan, M.P.: Investigation of powder mixed EDM of nickel-based superalloy using cobalt, zinc and molybdenum powders. Trans. Indian Inst. Met. 74(4), 923–936 (2021).
12. Boopathi, S.: Performance improvement of eco-friendly near-dry wire-cut electrical discharge machining process using coconut oil-mist dielectric fluid. J. Adv. Manuf. Syst. 22(2), 339–358 (2023).
13. Sharma, S., Vates, U.K., Bansal, A.: Parametric optimization in die-sinking EDM of Nimonic 90 alloy using Taguchi-based GRA approach. World J. Eng. 18(1), 146–156 (2021).
14. Muthuramalingam, T.: Effect of diluted dielectric medium on spark energy in green EDM process using TGRA approach. J. Clean. Prod. 238, 117894 (2019).
15. Singaravel, B., Shekar, K.C., Reddy, G.G., Prasad, S.D.: Performance analysis of vegetable oil as dielectric fluid in electric discharge machining process of Inconel 800. Mater. Sci. Forum 978, 77–83 (2020).
16. Yemul, O.S., Kamble, R.D., Thamke, V.R., Patil, S.D., Dawane, B.S., Kodam, K.M.: Preparation of biodegradable bioepoxy resins from waste vegetable oil for sustainable development. J. Sci. Soc. Technol. 32(1–2), 34–41 (2016).
17. Dastagiri, M., Srinivasa Rao, P., Madar Valli, P.: Optimization of EDM process parameters by using heuristic approach. Mater. Today Proc. 5(13), 27036–27042 (2018).
18. Gupta, K., Gupta, M.K.: Developments in nonconventional machining for sustainable production: A state-of-the-art review. Proc. Inst. Mech. Eng. Part C J. Mech. Eng. Sci. 233(12), 4213–4232 (2019).
19. Baroi, B.K., Jagadish, Patowari, P.K.: A review on sustainability, health, and safety issues of electrical discharge machining. J. Braz. Soc. Mech. Sci. Eng. 44(2), 59 (2022).
20. Jose, M., Sivapirakasam, S.P., Surianarayanan, M.: Analysis of aerosol emission and hazard evaluation of electrical discharge machining (EDM) process. Ind. Health 48(4), 478–486 (2010).
21. Elaiyarasan, U., Satheeshkumar, V., Senthilkumar, C., Nandakumar, C.: Mathematical and artificial neural network model in composite electrode assisted electrical discharge coating. Surf. Topogr. Metrol. Prop. 10(2), 025004 (2022).
22. Natarajan, U., Suganthi, X.H., Periyanan, P.R.: Modeling and multiresponse optimization of quality characteristics for the micro-EDM drilling process. Trans. Indian Inst. Met. 69(9), 1675–1686 (2016).

23. Ghoreishi, M., Tabari, C.: Investigation into the effect of voltage excitation of pre-ignition spark pulse on the electro-discharge machining (EDM) process. Mater. Manuf. Process. 22(7–8), 833–841 (2007).
24. Voigt, O., Peuker, U.A.: Suitability of eroded particles from die-sink electro discharge machining for additive manufacturing—review, characterization and processing. Metals 12(9), 1447 (2022).
25. Bhattacharya, A., Batish, A., Kumar, N.: Surface characterization and material migration during surface modification of die steels with silicon, graphite and tungsten powder in EDM process. J. Mech. Sci. Technol. 27(1), 133–140 (2013).
26. Agrawal, J.P., Somani, N., Gupta, N.K.: A systematic review on powder-mixed electrical discharge machining (PMEDM) technique for machining of difficult-to-machine materials. Innov. Emerg. Technol. 11, 2440002 (2024).
27. Govindan, P., Joshi, S.S.: Experimental characterization of material removal in dry electrical discharge drilling. Int. J. Mach. Tools Manuf. 50(5), 431–443 (2010).
28. Gevorkyan, E.S.: Remanufacturing and Advanced Machining Processes for New Materials and Components. Taylor & Francis, Boca Raton (2022).
29. Sharma, S., Dvivedi, A.: On material removal analysis of simultaneous electrochemical and electrodischarge machining process through analytical, numerical and experimental approaches. J. Manuf. Process. 135, 204–215 (2025).
30. Mahdieh, M.S.: Recast layer and heat-affected zone structure of ultra-fined grained low-carbon steel machined by electrical discharge machining. Proc. Inst. Mech. Eng. Part B J. Eng. Manuf. 234(5), 933–944 (2020).
31. Li, X., Wei, D., Li, Q., Yang, X.: Study on effects of electrode material and dielectric medium on arc plasma in electrical discharge machining. Int. J. Adv. Manuf. Technol. 107(11–12), 4403–4413 (2020).
32. Yadav, R.N.: Electro-chemical spark machining–based hybrid machining processes: Research trends and opportunities. Proc. Inst. Mech. Eng. Part B J. Eng. Manuf. 233(4), 1037–1061 (2019).
33. Nadda, R., Nirala, C.K., Singh, P.K., Lee, D., Kumar, R., Singh, T.: An overview of techniques for monitoring and compensating tool wear in micro-electrical discharge machining. Heliyon 10(6), e26784 (2024).
34. Tufail, M.S., Giri, J., Makki, E., Sathish, T., Chadge, R., Sunheriya, N.: Machinability of different cutting tool materials for electric discharge machining: A review and future prospects. AIP Adv. 14(4), 040702 (2024).
35. Volosova, M.A., Okunkova, A.A., Fedorov, S.V., Hamdy, K., Mikhailova, M.A.: Electrical discharge machining non-conductive ceramics: Combination of materials. Technologies 8(2), 32 (2020).
36. Uthirapathi, E., Chinnamuthu, S., Kaliyamoorthi, N.: An examination on dry sliding wear behaviour of AA7075 aluminium alloy modified with FA/Cu electro-discharge coating. J. Bio Tribo Corros. 10(2), 25 (2024).
37. Garba, E. et al.: A review of electrode manufacturing methods for electrical discharge machining: Current status and future perspectives for surface alloying. Machines 11(9), 906 (2023).